

Cyber Attacks Detection, Prevention, and Source Localization in Digital Substation Communication using Hybrid Statistical-Deep Learning

Nicola Cibir, Bas Mulder, Herman Carstens, Peter Palensky, Alexandru Ștefanov

Abstract—The digital transformation of power systems is accelerating the adoption of IEC 61850 standard. However, its communication protocols lack built-in authentication and encryption, leaving them vulnerable to Man-in-the-Middle (MitM) and malicious frame injection attacks that can disrupt protection schemes operation. While most existing research focuses on detecting cyber attacks in digital substations, intrusion prevention systems have been largely overlooked due to concerns about potential network disruptions. To address this gap, this paper proposes an integrated hybrid statistical-deep learning method for detecting, preventing, and localizing IEC 61850 Sampled Values (SV)-based cyber attacks. The method models SV frames arrival times using exponentially modified Gaussian distributions and prevents malicious frames from reaching the targeted Intelligent Electronic Devices (IEDs). Malicious frames are dropped with minimal processing overhead and latency, while the method remains robust to network latency, jitter, and time-synchronization issues, and ensures a near-zero false positive rate under non-attack conditions. Long short-term memory and Elman recurrent neural networks are used to identify anomalous variations in the estimated probability distributions across IEDs for detecting and localizing MitM attacks on SV streams. The proposed method is validated across three testbeds comprising industrial-grade communication and protection devices, hardware-in-the-loop simulations, virtualized IEDs and merging units, and high-fidelity emulated networks. Results demonstrate the method's practicality and effectiveness for deployment in IEC 61850-compliant digital substations.

Index Terms—Cyber Attacks, Deep Learning, Digital Substations, IEC 61850 Sampled Values, Intrusion Detection and Prevention System, Statistical Analysis.

I. INTRODUCTION

As proved by the latest cyber attacks on Ukraine's power grid in 2015, 2016, and 2022 [1]–[3], and the attempted one on the United Kingdom's power grid in 2020 [4], it is crucial to provide Industrial Control Systems (ICS), and, in broader terms, Operational Technology (OT) infrastructures, with state-of-the-art cyber security controls to ensure a secure

and resilient power system operation. The growing integration of Information Technology (IT) and OT infrastructures enables efficient power system operation and management. However, it also expands the attack surface and increases the risk of cyber attacks by introducing new cyber security threats [5].

Communication protocols defined in IEC 61850 standard have been developed to support advanced protection, automation, and control in digital substations. However, IEC 61850 inherently lacks fundamental network security mechanisms such as authentication and encryption. This deficiency is especially evident in the IEC 61850 Sampled Values (SV) protocol, where the absence of cryptographic protection allows malicious actors to inject forged frames into the substation OT communication network, potentially leading to major disruptions such as delayed fault clearance or unintended circuit breaker operations. Furthermore, these OT disruptions can affect power system stability, cause cascading failures and lead to large-scale outages or even a complete blackout [6], [7].

Several works in the literature have proposed the adoption of authentication and encryption to secure SV frames [8]–[12]. However, cryptographic schemes raise several challenges and limitations, including additional computational load, communication latency, message overhead, and increased infrastructure complexity. Another viable option to enhance cyber security in digital substation is the deployment of Intrusion Detection and Prevention Systems (IDSs and IPSs, respectively) [13]. Multiple studies have proposed intrusion detection methods based on the current and voltage measurements reported in SV frames [14]–[17]. Nonetheless, a key limitation of these IDSs is that relying solely on reported measurements can be misleading during replay attacks, in which normal operating conditions are re-injected by the attacker. In such cases, the measurements appear consistent with the physical model used for validation, and SV attack detection fails. To overcome this limitation, other authors have proposed IDSs that consider communication network traffic and SV frames header, relying on information such as the number of SV frames received each second (FS), the value of the `smpCnt` field, and the Inter-Frame Arrival Time (I-FAT) [17]–[24]. While these latest detection methods can effectively identify basic SV injection attacks, they fail against more sophisticated attacks, such as replay with spoofing and Man-in-the-Middle (MitM). In particular, when an attacker compromises a forwarding device, blocks the legitimate SV stream, and injects a malicious one, detection becomes infeasible because the attacker can simultaneously maintain the expected SV frames publishing

TABLE I: SV frames features used for cyber attacks detection.

	PHY	FS	smpCnt	I-FAT	F _{as}
Ustun et al. [14]	✓	✗	✗	✗	✗
Mo et al. [15]	✓	✗	✗	✗	✗
El Hariri et al. [16]	✓	✗	✗	✗	✗
Hussain et al. [17]	✓	✗	✓	✗	✗
Hong et al. [18]	✗	✓	✓	✗	✗
Delhomme et al. [19]	✗	✗	✓	✓	✗
Wannous et al. [20]	✗	✓	✗	✓	✗
Hong et al. [21], [24]	✗	✓	✓	✗	✗
Eynawi et al. [22]	✓	✗	✗	✓	✗
Manzoor et al. [23]	✓	✗	✓	✗	✗
Our Solution	✗	✓	✓	✓	✓

rate (FS), increment the `smpCnt` field consistently, spoof the SV stream identifier, and closely match the expected inter-frame arrival timing. Moreover, the time required to detect the attacks ranges from a few hundred microseconds [14] to hundreds of milliseconds [23], depending on the available computational power and the implemented detection method. For these reasons, existing approaches cannot be applied for real-time intrusion prevention, MitM attacks detection, and malicious device localization. Finally, none of the existing works exploits the informative advantage provided by the statistical properties of the SV frames arrival time shift (F_{as}) to detect, prevent, and localize SV-based injection attacks, which is one of the contributions of this paper, as summarized in Table I.

While existing works focused on intrusion detection, the deployment of IPSs in digital substations has so far received limited attention, mainly due to a general reluctance to adopt such solutions in OT infrastructures. This reluctance primarily stems from the risk of potential disruptions to time-critical OT communication networks in digital substations, including increased latency, packet loss, and additional computational overhead. Nevertheless, detection alone is not sufficient to ensure resilient power system operation. Even when an attack is promptly identified, its impact on protection and control functions may already have occurred. Therefore, proactive intrusion prevention mechanisms are essential to mitigate or entirely avoid undesired consequences before they propagate through the OT system, while ensuring no interference with protection, automation, and control functionalities.

To address these gaps, this paper proposes an integrated method for detecting, preventing, and localizing the source of IEC 61850 SV cyber attacks in digital substations, aiming to enhance both situational awareness and operational security while meeting real-time communication requirements for protection schemes. The main contributions of this paper are summarized as follows:

- 1) We present the first integrated method combining statistical modeling and Deep Learning (DL) for real-time detection, prevention, and source localization of IEC 61850 SV cyber attacks in digital substations. The method introduces a novel analytical formulation of SV frames arrival times statistics using Exponentially Modified Gaussian (EMG) probability distributions to accurately model network latency, jitter, and device clock drift during time synchronization loss. The combination of the statistical

approach with DL enables the identification and mitigation in real-time of MitM and all known techniques of SV injection attacks.

- 2) We employ Long Short-Term Memory (LSTM) models to capture temporal deviations in the estimated probability distributions, enabling timely detection of ongoing MitM attacks on SV streams against the protected Intelligent Electronic Devices (IEDs).
- 3) We adopt Elman Recurrent Neural Networks (RNNs) to combine and correlate the estimated probability distribution across multiple IEDs within High-availability Seamless Redundancy (HSR) rings. By analyzing the spatio-temporal correlations among Probability Distribution Functions (PDFs), the compromised device used to perform the MitM attack on SV streams can be precisely localized.
- 4) We utilize the estimated PDFs to discern legitimate and malicious frames in real-time, allowing malicious frames to be discarded before affecting IED protection logic. This provides an effective intrusion prevention mechanism with minimal processing overhead and high operational explainability.
- 5) We validate the proposed method for real-time detection, prevention, and source localization of IEC 61850 SV cyber attacks in digital substation on two lab testbeds and an industrial testbed at Elia transmission system operator in Belgium comprising industrial-grade protection and communication devices, hardware-in-the-loop simulations, virtualized IEDs (vIEDs) and merging units (vMUs), and high-fidelity emulated OT networks. Results demonstrate accurate detection and localization of MitM attacks on SV streams, reliable filtering of forged SV frames, a near-zero False Positive Rate (FPR) in the absence of cyber attacks, negligible additional latency, and throughput exceeding 100,000 SV frames per second. The method remains resilient to communication latency, jitter, and time synchronization deviations, making it suitable for deployment in IEC 61850-based digital substations.

The remainder of the paper is organized as follows. In Section II, background information about the SV protocol and cyber security concerns is provided. In Section III, the integrated method proposed for the detection, prevention, and source localization of IEC 61850 SV-based cyber attacks is presented. In Section IV, the proposed method is extensively validated, evaluated, and compared with the related state-of-the-art solutions. Finally, Section V concludes the paper.

II. BACKGROUND

As introduced in the previous sections, the operation of digital substations relies on time-critical communication services defined within the IEC 61850 standard. Understanding both the operational principles of the SV protocol and its associated cyber security requirements is essential for assessing vulnerabilities and designing effective defence mechanisms. The following subsections first provide an overview of the IEC 61850 SV protocol and its deterministic timing characteristics, followed by a discussion on the security challenges and countermeasures proposed in the relevant IEC standards.

A. IEC 61850 Sampled Values

IEC 61850 SV is a publisher-subscriber protocol used for three-phase current and voltage measurements reporting from Merging Units (MUs) to IEDs. MUs publish SV frames in multicast, whereas IEDs process only the SV streams to which they are subscribed. The protocol was initially introduced in IEC 61850-9-2, further refined in IEC 61850-9-2LE, and ultimately standardized in IEC 61869-9. Various SV frame publishing rates are specified based on system frequency and application requirements. In digital substations, the most used rates are 4000 and 4800 frames per second for 50 Hz and 60 Hz power systems, respectively. Additionally, the standard defines the structure of SV frames, including the `smcCnt` field, a counter that increments with each published frame and resets to zero every second. Consequently, the `smcCnt` value ranges from zero to the number of frames published each second minus one. This part of the standard provides a certain level of determinism on the specific arrival time of each of the SV frames marked with a specific `smcCnt` value. In fact, given a specific second i , a predefined number of frames per second FS , and a `smcCnt` field value c , the theoretical frame arrival time $F_a^e(i, c)$ is computed as follows:

$$F_a^e(i, c) = i + c \cdot \frac{1}{FS}, \quad \forall c \in \{0, 1, \dots, FS - 1\} \quad (1)$$

This theoretical determinism in the frames' arrival time across publishing periods provides an information advantage to discern legitimate and malicious SV frames, detect MitM attacks, and locate compromised IEDs within the OT communication network. To further increase the determinism of the SV frames arrival time, as recommended in IEC 61850-90-4, priority tags and proper communication network engineering should be used to ensure the lowest possible latency and jitter for SV frames [25].

B. Sampled Values Cyber Security

Considering the strict latency requirements of power system protection schemes of 3 ms, the IEC 62351 standard stipulates against the application of digital signatures due to increased latency and processing times. To counteract most of the possible cyber attacks exploiting the SV protocol, the standard recommends the usage of Message Authentication Codes (MAC) relying on Hash-based MAC (HMAC) or Advanced Encryption Standard-Galois MAC (AES-GMAC) to provide message authentication. While appending the computed MAC to published frames helps mitigate replay, spoofing, and MitM attacks, it also introduces multiple challenges and limitations. These include the increased publishing and subscribing devices computational load, communication latency, and message overhead, the need for Public Key Infrastructure (PKI) and multiple Key Distribution Centers (KDCs) deployment, lack of support for legacy devices not supporting IEC 62351-6, and the risk of pre-shared keys violation. Moreover, each device belonging to the same Group Domain of Interpretation (GDOI) has access to the same shared secret key, and thus can perform spoofing attacks.

Summarizing, once an attacker is able to gain access to the digital substation OT communication network [5], the

cyber attacks that can be performed against an SV subscriber include: (1) flooding, where a large number of SV frames are injected into the communication network by the attacker to exhaust subscriber resources; (2) spoofing, where the attacker injects malicious SV frames pretending of being the legitimate SV publisher; (3) replay, where the attacker re-injects into the communication network the previously sniffed SV frames; (4) high `smcCnt` attack, in which an attacker injects one or multiple SV frames with a high `smcCnt` field value, causing the SV subscriber implementing the replay protection mechanism as mandated in IEC 62351-6 to discard any further legitimate SV frame with a lower `smcCnt`; (5) MitM, where an attacker takes control of a device forwarding SV frames from the publisher to the subscriber and tampers with the forwarded SV frames; (6) access to the pre-shared secret key, in which the attacker gains access to the pre-shared secret key used for MAC generation and validation and injects authenticated malicious SV frames.

In this paper, to evaluate the effectiveness of the proposed method, the performed cyber attacks assume the injection of malicious SV frames that are completely indistinguishable from the legitimate ones. In other words, the Hamming distance between the content of legitimate and malicious SV frames is equal to zero. By proving the method's effectiveness in this worst-case scenario, the results can be extended to cases where false measurements are injected, thus leading to a Hamming distance greater than 0.

III. CYBER ATTACKS DETECTION, PREVENTION, AND SOURCE LOCALIZATION

The proposed integrated method can be divided into two main modules, i.e., (1) the intrusion detection and prevention module, which is deployed in each IED, and (2) the attack source localization module, which is deployed on a centralized location within the digital substation and receives statistical information from each IED. Fig. 1 represents the architecture of the proposed method. In the following, theoretical preliminaries and the different components and their interactions are presented.

A. SV Frames Arrival Time Shift

As introduced in Section II, the IEC 61869-9 standard mandates strict timing specifications for SV publishers. Given that in real communication networks, the theoretical frame arrival time is affected by frame transmission, propagation, queuing, and processing delays, and time synchronization errors among SV stream publisher and subscriber devices, each frame is received at a time $F_a^r(c) \neq F_a^e(c)$, within each second. By monitoring the SV subscriber's Network Interface Card (NIC), the arrival time $F_a^r(c)$ of each received frame can be measured, and consequently, the difference between the theoretical and empirical frame arrival times can be computed as shown in (2).

$$F_{as} = F_a^r(c) - F_a^e(c), \quad \forall c \in \{0, 1, \dots, FS - 1\} \quad (2)$$

To account for the stochasticity of the communication network infrastructure, a PDF can be estimated over F_{as} . Then,

the modeled PDF can be used as an information advantage for intrusion detection, prevention, and attack source localization. Indeed, once this PDF is estimated, a legitimacy probability can be assigned to each received frame, allowing the distinction between legitimate and malicious SV frames based on their F_{as} measured at the subscriber. Regarding the choice of the most appropriate PDF to be used, the literature shows that latency in communication networks is often modeled using an exponential distribution [26]. However, the exponential distribution assigns a probability equal to zero to samples below its lower bound, making it unsuitable for scenarios where latency reductions may occur due to device time-synchronization errors. To address this limitation, the EMG distribution is used to model F_{as} . The EMG, defined as the sum of a Gaussian and an exponential component, effectively represents both the narrow, near-deterministic base communication delay and the heavy-tailed positive jitter caused by queueing, contention, and background traffic. Such characteristics enable the EMG to capture the sharp mode and long right tail observed in empirical network latency distributions more accurately than either distribution alone.

Finally, it should be remarked that, while related, the inter-frame arrival time, i.e., I-FAT, and SV frames arrival time shift, i.e., F_{as} , differ fundamentally in definition, probability distribution, information content, and susceptibility to communication network latency and jitter. In fact, I-FAT represents the time difference between consecutive SV frames and follows a Gaussian distribution centered at $1/FS$, whereas F_{as} measures the deviation between the expected and actual arrival times for individual frames, modeled by an EMG distribution whose mean reflects communication network latency and clock synchronization drift [27]. These distinctions represent a fundamental difference compared to how the SV frame arrival times information has been exploited in existing studies.

B. Exponentially Modified Gaussian Distribution

The EMG distribution is a probability distribution whose PDF is obtained by convoluting a normal distribution, $Z \sim \mathcal{N}(\mu, \sigma^2)$, with an exponential one, $E \sim \text{Exp}(\lambda)$. An EMG distribution is characterized by the following PDF:

$$f_{EMG}(x) = \frac{\lambda}{2} e^{\frac{\lambda}{2}(2\mu + \lambda\sigma^2 - 2x)} \text{erfc}\left(\frac{\mu + \lambda\sigma^2 - x}{\sqrt{2}\sigma}\right) \quad (3)$$

where μ and σ are the mean and standard deviation of the normal distribution, respectively, and $\lambda = 1/\tau$ is the exponential decay of the exponential distribution. Due to the changing operating conditions, F_{as} can vary in time, and thus EMG distribution parameters need to be continuously estimated and updated using the latest received SV frames. As shown by Ali et al. [28], the Method of Moments Estimation (MME) provides the best trade-off in terms of parameters estimation accuracy and efficiency. In fact, to minimize SV frames classification latency, an accurate estimator providing a closed form solution is required. By using the MME, it is possible to equate the first three theoretical moments of the EMG distribution with the three empirical ones as in (4), (5),

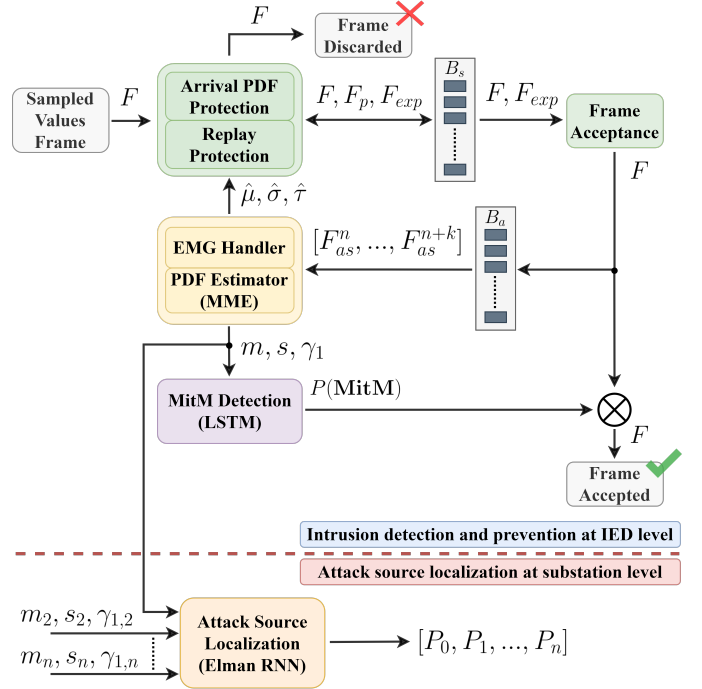


Fig. 1: Hybrid statistical-deep learning-based intrusion detection, prevention, and attack source localization system architecture.

and (6), for the mean (m), variance (s^2), and skewness (γ_1), respectively:

$$\mathbb{E}[X] = m = \mu + \tau = \hat{m}_1 \quad (4)$$

$$\text{Var}(X) = s^2 = \sigma^2 + \tau^2 = \hat{m}_2 \quad (5)$$

$$\gamma_1 = \frac{2\tau^3}{(\sigma^2 + \tau^2)^{3/2}} = \frac{\hat{m}_3}{\hat{m}_2^{3/2}} \quad (6)$$

where \hat{m}_r is the r -th empirical moment computed on the observed data. As shown in Oliver et al. [29], solving for the EMG distribution parameters gives:

$$\hat{\mu} = m - s \left(\frac{\gamma_1}{2}\right)^{1/3} \quad (7)$$

$$\hat{\sigma}^2 = s^2 \left[1 - \left(\frac{\gamma_1}{2}\right)^{2/3}\right] \quad (8)$$

$$\hat{\tau} = \frac{1}{\hat{\lambda}} = s \left(\frac{\gamma_1}{2}\right)^{1/3} \quad (9)$$

where $\hat{\mu}$, $\hat{\sigma}$, and $\hat{\lambda}$ are the estimated PDF parameters.

C. Intrusion Detection and Prevention

To discern legitimate and malicious SV frames on a per-frame basis in real-time, and to detect MitM attacks, the proposed method relies on four interdependent components being executed in parallel in each IED. Moreover, two buffers, i.e., the staging buffer (B_s) and the accepted frames buffer (B_a), are used to store the latest received frames which are most likely to be legitimate, and the last k accepted frames, respectively.

1) *Arrival PDF and Replay Protections*: Once a new SV frame is received at the subscriber NIC, it is processed by the first component. First, it is checked whether frames with the same `smcCnt` value were already accepted in the current time period. If it is the case, the replay protection mechanism is triggered, and the frame is discarded. Then, after computing F_{as} for the current frame as presented in the previous section, the EMG PDF (f_{EMG}) is used to compute the probability of the frame being legitimate (F_p), such that $F_p = f_{EMG}(F_{as})$. Subsequently, the component checks whether in B_s a frame with the same `smcCnt` value as the just received frame is present. If such a frame is already present, but the probability of it being legitimate is higher than the one computed on the last received frame, the last received frame is discarded. Otherwise, if no frame with the same `smcCnt` is present in B_s , or the legitimacy likelihood of the new frame is higher, the just received frame is inserted in the buffer, and the already present one is discarded. In this way, it is ensured that exactly FS frames per second are accepted and no false positives can occur when no cyber attack is ongoing. Other than computing F_p , a frame expiration time (F_{exp}) is assigned to each frame added to B_s , with F_{exp} computed as follows:

$$F_{exp} = \begin{cases} 0, & F_{as} \geq \mathbb{E}[F_{as}]^t \\ F_a + r, & F_p \geq f_{EMG}(\mathbb{E}[F_{as}]^t) \\ F_a + r + 3 \cdot \hat{\sigma}^t, & \text{otherwise} \end{cases} \quad (10)$$

where the residual r is equal to $\mathbb{E}[F_{as}]^t - F_{as}$.

The rationale behind the values assigned to F_{exp} is to minimize the time frames remain buffered in B_s while ensuring that frames with the highest likelihood of originating from the legitimate device, rather than from the attacker, are accepted. In fact, if a frame with `smcCnt` equal to c is received at time F'_a , and the computed F'_{as} is equal to or greater than $\hat{\mu}^t + \hat{\tau}^t = \mathbb{E}[F_{as}]^t$, then, for any other frame with the same `smcCnt` received at a time $F''_{as} > F'_{as}$, $f_{EMG}(F''_{as}) = F''_p$ will be lower than $f_{EMG}(F'_{as}) = F'_p$. Thus, the frame can be accepted immediately without any further delay. In the other cases, it cannot be inferred that frames with higher legitimacy likelihood will not be received in the future, and thus the received frame needs to be retained until F_{exp} . A graphical interpretation on the values assigned to F_{exp} is provided in Fig. 2. Moreover, the pseudocode for this component is provided in Algorithm 1.

2) *Frame Acceptance*: This component is responsible for processing SV frames stored in B_s , while continuously mon-

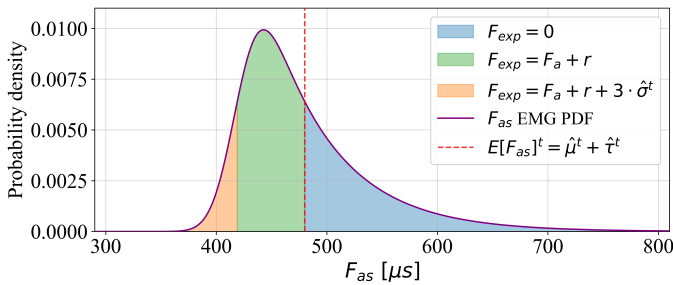


Fig. 2: Graphical interpretation of F_{exp} value assignment.

Algorithm 1: SV frame likelihood (F_p) and expiration (F_{exp}) computation, and push frame to staging buffer.

Input : SV frame F , Frame arrival time shift (F_{as}),
Current buffer B_s

Output: Updated buffer B_s or Discard frame

```

1 if  $|F_{as} - \mathbb{E}[F_{as}]^t| \geq 3 \cdot \hat{\sigma}^t$  then
2   Discard  $F$ 
3   Return
4  $F_p \leftarrow f_{EMG}(F_{as})$ 
5 if  $F_{as} \geq \mathbb{E}[F_{as}]^t$  then
6    $F_{exp} \leftarrow 0$ 
7 else if  $F_p \geq f_{EMG}(\mathbb{E}[F_{as}]^t)$  then
8    $F_{exp} \leftarrow F_a + (\mathbb{E}[F_{as}]^t - F_{as})$ 
9 else
10   $F_{exp} \leftarrow F_a + (\mathbb{E}[F_{as}]^t - F_{as}) + 3 \cdot \hat{\sigma}^t$ 
11  $F_{new} \leftarrow \{F, F_p, F_{exp}\}$ 
12 if  $\exists F' \in B_s$  s.t.  $F'_{smcCnt} == F_{smcCnt}$  then
13   if  $F'.F_p < F_p$  then
14     Replace  $F'$  with  $F_{new}$  in  $B_s$ 
15   else
16     Discard  $F$ 
17 else
18   Insert  $F_{new}$  into  $B_s$  maintaining order by  $smcCnt$ 
19 Return
```

itoring whether the current time is higher than frames' F_{exp} . If this condition holds, it implies that no additional SV frames with the same `smcCnt` field value and a higher likelihood of legitimacy are expected to be received. Thus, the SV frame currently stored in B_s can be accepted, forwarded to the protection scheme for immediate use, and added to B_a , which stores the SV frames used for updating the parameters of the EMG PDF.

3) *EMG Handler and PDF Estimator*: After the number of SV frames in B_a is greater than k , this component takes care of estimating and updating the parameters of the EMG distribution. This is done by first updating the samples' moments with a weighted mean between the previously calculated moments (\hat{m}_r^t) and the just computed ones (\hat{m}_r), as in (11), and then using the updated moments values to compute the updated EMG parameters $\hat{\mu}^{t+1}$, $\hat{\sigma}^{t+1}$, and $\hat{\lambda}^{t+1}$.

$$\hat{m}_r^{t+1} = \frac{FS \cdot \hat{m}_r^t + k \cdot \hat{m}_r}{FS + k} \quad (11)$$

The updated EMG parameters are then used by the arrival PDF and replay protections component to evaluate the legitimacy of any SV frame that arrived subsequently.

4) *MitM Detection*: Whereas the first component is meant to accept exactly FS SV frames per second while minimizing the likelihood of malicious frames being accepted, this fourth component aims at detecting MitM attacks on SV streams. In this type of attack, the attacker can completely block the legitimate SV stream and inject a malicious one by compromising one forwarding device between the SV publisher and subscriber. Thus, the subscriber device receives exactly FS

frames per second as expected. Still, as experimentally shown, the act of intercepting and tampering with the forwarded SV frames causes an inevitable change in the latency and jitter statistics of the received SV stream at the subscriber level. In fact, to perform the MitM attack, the attacker is required to change the NIC configuration of the compromised forwarding device to modify the frames forwarding rules or to disable the HSR bridge between the two NICs. Then, the network traffic needs to be monitored, tampered with, and forwarded from one NIC to the other in user-space level on the device, causing the inevitable alteration of the forwarded traffic statistical properties. A RNN is deployed to detect anomalous variations in the EMG parameters. The input of the RNN consists of the mean (m), standard deviation (s), and skewness (γ_1) of the F_{as} measured on the accepted frames, calculated over a sliding window of 200 samples with a step size of 50 samples. The RNN outputs the likelihood of an ongoing MitM attack. A grid search approach is used to select the most appropriate RNN model and perform hyperparameter optimization. The considered RNN models include Elman RNN, LSTM, and Gated Recurrent Units (GRU), whereas the dimension and the number of hidden layers vary from 3 to 20 and from 2 to 8, respectively. The model providing the best trade-off between model complexity, detection accuracy, and prediction time consists of 4 stacked LSTM cells of 20 neurons each. Finally, to perform the binary classification, a fully connected layer is stacked to the output of the last LSTM cell.

D. Attack Source Localization

As mentioned in the previous section, anomalous changes in the PDF of F_{as} can be an indicator of an ongoing MitM attack. By aggregating and correlating the statistical properties of the SV frames arrival times from different IEDs deployed within the digital substation, it is possible to identify and locate which device is performing a MitM attack. In this paper, the focus is on IEDs deployed in an HSR ring topology. As represented in Fig. 1, the mean (m_i), standard deviation (s_i), and skewness ($\gamma_{1,i}$) of the measured F_{as} from each i -th IED are delivered to the server hosting the attack source localization module within the digital substation. These metrics are then used to estimate the probability of a MitM attack being ongoing, and the probability for each IED of acting maliciously. As for the MitM component, a sliding window of 200 F_{as} samples with a step size of 50 samples is used. This last component consists of 5 stacked Elman RNN cells; each cell hidden layer contains 26 neurons. The tanh activation function is used. The output of the last RNN cell is provided as input to a fully connected layer to perform the final multi-class classification. To improve the DL model accuracy and increase its generalization capabilities, the component's input data is derived from the statistical metrics received from each IED as follows:

$$\forall t \in \{1, \dots, T\}, \forall i, j \in \{1, \dots, N\}, i < j :$$

$$\begin{cases} m_{i,j}^t = m_i^t - m_j^t \\ s_{i,j}^t = s_i^t - s_j^t \\ \gamma_{1,i,j}^t = \gamma_{1,i}^t - \gamma_{1,j}^t \end{cases} \quad (12)$$

where t is the current time window, N is the number of IEDs deployed in the HSR ring, and m_n^t , s_n^t , and $\gamma_{1,n}^t$ are the mean, standard deviation, and skewness measured at n -th IED at time t . This data transformation prevents the DL model from overfitting the absolute values measured in the specific communication network conditions, but to focus on the relative evolution of the statistical properties.

E. Attacker Considerations

From an attacker's perspective, several challenges need to be overcome to deceive the proposed intrusion detection and prevention method. First, estimating F_{as} for a specific SV subscriber from a different device in the network requires the estimation of the overall communication latency between the legitimate publisher and the targeted subscriber, and between the compromised device and the targeted subscriber. Furthermore, this estimation needs account for timing synchronization errors. Second, to inject the SV frames at the exact time instant required to match the expected F_{as} , the compromised device needs to be executing a real-time operating system and be time synchronized with Precision Time Protocol (PTP). Moreover, to carry out the attack, a malicious script capable of publishing SV frames must be delivered, installed, and executed with high privileges on the compromised device. This deployment must occur stealthily, avoiding detection by both host-based and network-based IDSs; also, the script execution should not exhaust compromised device resources. Finally, to cause protection schemes to react to a fault, it is not sufficient to have only a small number of false measurements to be accepted. For instance, when overcurrent protection is implemented, the measured current needs to be above a certain threshold for at least 200 ms. This means that an attacker needs at least $FS/5$ consecutive malicious frames to be accepted to trigger the protection scheme. Thus, the injected malicious frames need to be consistently accepted for a non-negligible amount of time. The combination of these conditions imposes considerable complexity on potential attacks, effectively preventing successful deception of the proposed method, even under ideal scenarios. In the remainder of the paper, it is assumed that the attacker has gained privileged access to a machine connected to the network switch forwarding the legitimate SV stream, or to a forwarding device itself when considering MitM attacks, and can execute arbitrary scripts with high privileges to directly access the compromised machine's NIC and inject malicious SV frames.

IV. EXPERIMENTAL RESULTS AND DISCUSSION

The proposed method was extensively tested on data acquired from three different IEC 61850-compliant testbeds. The first testbed consists of a Real-Time Digital Simulator (RTDS) simulating an IEEE 5-bus system, a GTNETx2 card acting as an SV publisher and GOOSE subscriber, a network switch, and three vIEDs connected to the network switch in a hardware-in-the-loop configuration, acting as SV subscribers. The second testbed is deployed by Elia transmission system operator in Belgium and consists of industrial-grade devices deployed in a Parallel Redundancy Protocol (PRP) configuration. In this

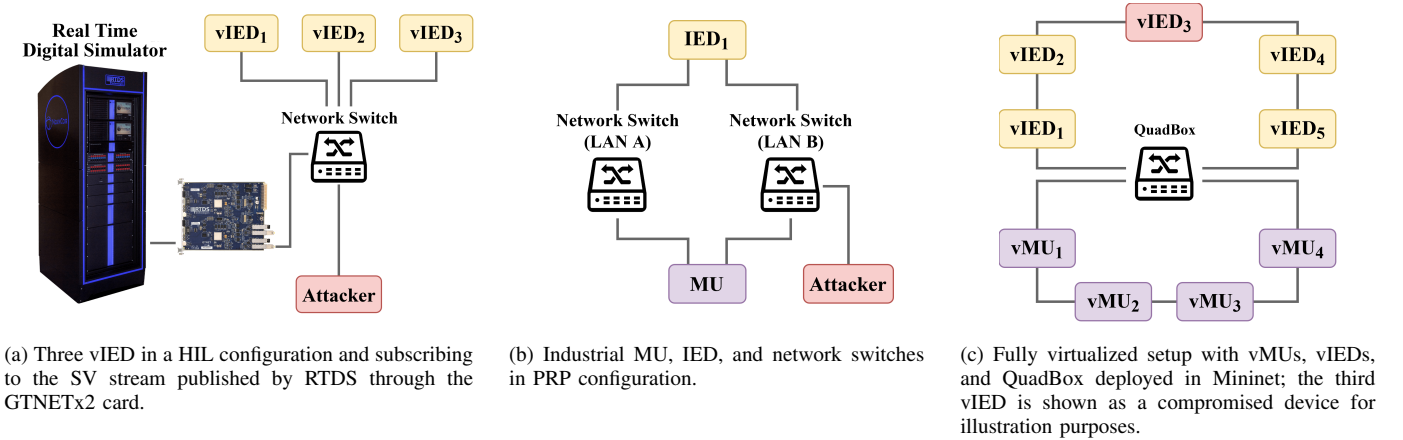


Fig. 3: Schematic overview of the three experimental testbeds used to validate the proposed method.

second case, the deployed devices include an industrial MU publishing an SV stream, two IEC 61850-compliant network switches, and an IED. Finally, the third testbed consists of a fully virtualized setup in which the digital substation communication network was emulated in Mininet. The setup consists of two HSR rings, connected through a QuadBox, and containing 4 vMUs and 5 vIEDs, respectively. Fig. 3 depicts the architecture of the three testbeds.

The experiments in the first testbed involved both SV injection attacks from a compromised device connected to the network switch and MitM attacks against one vIED. The second testbed focused exclusively on SV injection attacks from a compromised device connected to one of the network switches. Finally, the third testbed was dedicated to performing MitM attacks from each vIED in the HSR ring, one at a time. During SV injection attacks, the attacker injected malicious measurements while spoofing the identity of the legitimate SV publisher, emulating persistent false fault conditions that triggered the (v)IEDs to incorrectly issue trip commands for opening circuit breakers. The IPS aimed to block these malicious SV frames from reaching the protection scheme while minimizing the drop of legitimate traffic. MitM attacks against the vIEDs verified that changing NIC configuration and forwarding and tampering SV frames in user-space through a highly optimized C script would still cause detectable changes in the statistical distribution of frame arrival times received by the targeted IED. Finally, data collected in the third testbed was used for training and testing the attack source localization module. In all cases, network traffic acquisitions were obtained by running Wireshark on each (v)IED and network switch across the three testbeds. Notably, the integrated method classified frames, detected MitM attack, and localized the compromised devices without inspecting measurement data, rendering differences between legitimate and malicious measurements irrelevant for this evaluation.

A. Frame Arrival Time Characterization

Fig. 4 illustrates how the EMG distribution aligns with the measured F_{as} values at one vIED deployed in the third testbed.

Also, Table II reports the Akaike's Information Criterion (AIC) normalized by sample size, the Bayesian Information Criterion (BIC), and the Kolmogorov-Smirnov (KS) test results computed on the monitored SV streams for one (v)IED for each testbed. As observed, the EMG distribution achieves a better fit than Gaussian and exponential distributions across all testbeds. It is acknowledged that an exhaustive search over alternative PDFs could identify models with improved fit for this particular dataset. Nevertheless, such an approach would risk overfitting and undermine the physical interpretability of the modeled data. Therefore, the EMG distribution was selected based on domain knowledge, balancing statistical fit with interpretability and relevance to substation communication patterns, rather than adopting a brute-force optimization strategy.

TABLE II: AIC, BIC, and KS test results for Gaussian, exponential, and EMG distributions fitted on SV streams on one (v)IED per testbed.

Testbed	PDF	AIC	BIC [$\times 10^3$]	KS
vIED ₁	Gaussian	11.35	454	0.271
	Exponential	10.46	418	0.328
	EMG	9.41	377	0.083
IED ₁	Gaussian	9.15	366	0.271
	Exponential	9.19	368	0.370
	EMG	8.22	329	0.167
vIED _{HSR}	Gaussian	12.03	24	0.223
	Exponential	10.77	22	0.103
	EMG	10.61	22	0.082

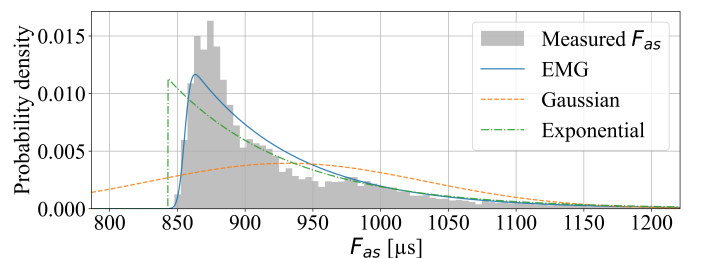


Fig. 4: Comparison of EMG, Gaussian, and exponential distribution fits to the measured F_{as} .

TABLE III: Information about the monitored SV streams at different (v)IEDs.

	vIED ₁	vIED ₂	vIED ₃	IED ₁
FS [$frames/s$]	4800	4800	4800	4000
$\mathbb{E}[F_{as}]$ [ms]	-7.08	-4.60	0.447	-113.30
F_{as} std. dev [μs]	53	123	104	25
Holdover [$\mu s/s$]	-1.399	1.658	-0.032	-0.371

The main information about the monitored SV streams in the first two testbeds during normal conditions is reported in Table III. This information includes the number of frames received per second (FS), measured F_{as} mean and standard deviation, and the overall time synchronization error due to the lack of time synchronization with the PTP master clock. It should be noted that to comply with IEC 61850-9-3, each IED should guarantee a maximum holdover of $\pm 0.2 \mu s/s$, thus implying a maximum time synchronization divergence among two devices of $\pm 0.4 \mu s/s$. Given the holdovers observed during our tests, it is reasonable to assert that the proposed method was evaluated under the most challenging conditions likely to be encountered in real digital substation environments.

B. Intrusion Prevention Evaluation

To effectively evaluate the performance of the proposed intrusion prevention method, the True Positive Rate (TPR), FPR, and F1-score metrics are considered. For a fair assessment, it is essential to keep into consideration and maximize the TPR while minimizing the FPR. This is because a considerable number of consecutive false negatives can lead the (v)IED to issue unintended control commands to circuit breakers. Conversely, if many legitimate SV frames are discarded because wrongly classified, the protection algorithm is prevented from operating properly and in a timely manner.

Before testing the IPS against SV injection attacks, its performance in terms of false positives during normal operating conditions is evaluated. During normal conditions, the IPS caused FPR of 0.07%, 0.35%, 0.32%, and 0.005% on vIED₁, vIED₂, vIED₃, and IED₁, respectively. These false positives were mainly caused by frames being received with an unexpected latency greater than 3 ms. Indeed, as can be noted in Table III, higher FPR resulted in (v)IEDs experiencing higher levels of communication jitter, i.e., higher variance of F_{as} . These frames exceed IEC 61850 latency limit of 3 ms and would be discarded by protection schemes, aligning with expected IPS behavior.

Subsequently, malicious SV streams were injected into the OT communication network from a compromised machine connected to the network switch in the first and second testbeds. Due to the attacker's challenges discussed in Section III-E, perfectly matching the expected F_{as} was not feasible. In fact, after several trials and adjustments, the minimum difference between the frame arrival time shift expected by the SV subscriber (F_{as}^{leg}) and frame arrival time shift of the frames injected by the attacker (F_{as}^{mal}) was $-178 \mu s$. The difference between F_{as}^{leg} and F_{as}^{mal} , which will be referred to as $F_{as}^{(mal-leg)}$, can be seen as the attacker's injection time

TABLE IV: IPS performances against SV injection attacks performed on the first two testbeds.

	vIED ₁	vIED ₂	vIED ₃	IED ₁
# Legitimate frames	43124	43124	43124	50000
# Malicious frames	19201	19201	19201	50000
$\mathbb{E}[F_{as}^{(mal-leg)}]$ [μs]	-178	-223	-205	1001
FPR [%]	0.67	0.42	0.77	0.005
TPR [%]	98.50	99.74	98.78	100
Precision [%]	98.49	99.07	98.28	100
F1-score [%]	98.49	99.41	98.53	100

shift error. As can be appreciated in Table IV, even with such small attacker injection time shift errors, the IPS provided FPRs lower than 0.77% and TPRs higher than 98.5%.

To accurately estimate the IPS performance as a function of $F_{as}^{(mal-leg)}$, a synthetic dataset was generated from the original one. In this synthetic dataset, the original legitimate frames were duplicated, and the F_{as} values of the duplicated frames were varied such that $F_{as}^{(mal-leg)}$ lies within $\pm 600 \mu s$. These duplicated frames represent the malicious frames injected by the attacker. This approach allows to accurately identify method's prevention boundaries by analyzing its performance in the relevant search space that reflects attacker capabilities.

As can be observed in Fig. 5, the IPS provided great prevention capabilities down to an attacker injection error of less than $\pm 100 \mu s$, with FPRs lower than 1% and F1-scores above 95%. Higher $F_{as}^{(mal-leg)}$ absolute values were not considered because they would lead to F1-scores close to 100%. As expected, the limitation of the proposed IPS comes into play when the attacker matches the expected legitimate F_{as} . In that case, the information advantage is lost, and legitimate and malicious frames have a 50% probability of being accepted or discarded. Final consideration regards the IPS added latency and throughput performances. Throughout

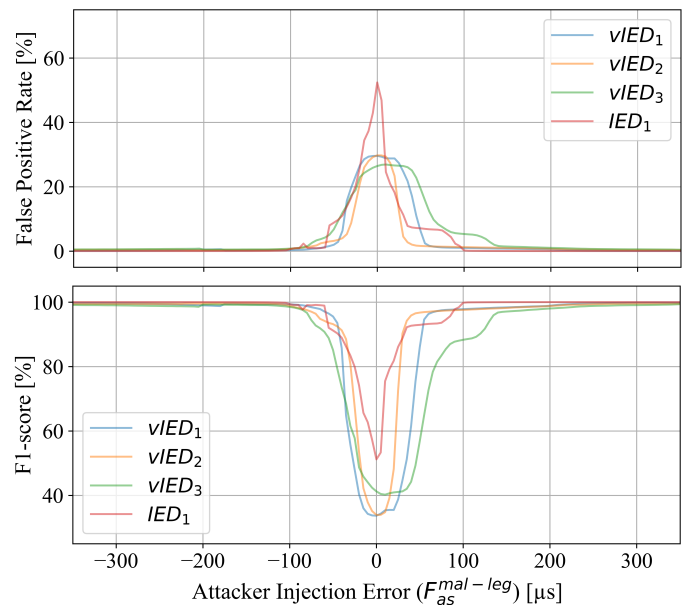


Fig. 5: FPR and F1-score of the intrusion prevention method as a function of attacker injection error on the four (v)IEDs deployed across the first and second testbeds.

the tests, it was verified that the IPS introduced an additional latency of around $150 \mu s$ and sustained a throughput exceeding 100,000 frames per second. These performances satisfy the stringent timing requirements specified in IEC 61850-5 and support the highest SV frames publishing rate of 96,000 frames per second, as defined in IEC 61869-9.

C. MitM Detection Evaluation

Experiments on the first testbed revealed that MitM attacks against a (v)IED produced significant changes in SV frame arrival-time statistics. Specifically, frame interception and tampering increased latency by $40.55 \mu s$, jitter by 8.48%, and PDF skewness by 115.79%, on average. These results demonstrate that SV frame arrival-time statistics provide a reliable indicator for MitM attack detection.

Consequently, the MitM attack detection component was evaluated on four synthetic datasets generated from the network traffic acquisitions from the first two testbeds, enabling the identification of the component's detection boundaries. The attacker, by compromising a forwarding device and performing a MitM attack against the subscriber, could drop the legitimate SV stream and inject a malicious one in real-time. As a result, the SV subscriber received exactly the expected number of SV frames, i.e., FS , but the statistical properties of their arrival times were altered due to the MitM attack. This expected behaviour was experimentally verified in the third testbed, where the MitM attacks were practically performed.

To generate the synthetic anomalous acquisitions, half of the legitimate data was modified by introducing variations in the mean, standard deviation, and skewness of the measured F_{as} . These variations are referred to as Δm , Δs , and $\Delta \gamma_1$, with values drawn from uniform distributions with lower and upper bounds of $\pm 300 \mu s$, $\pm 10\%$, and $\pm 5\%$, respectively. After selecting a detection threshold providing FPRs lower than 0.15% and 0.01% in the first and second testbeds, respectively, the MitM component provided TPRs of 95.15%, 95.99%, 93.85%, and 97.66%, for vIED₁, vIED₂, vIED₃, and IED₁, respectively. Still, it must be kept in consideration that in

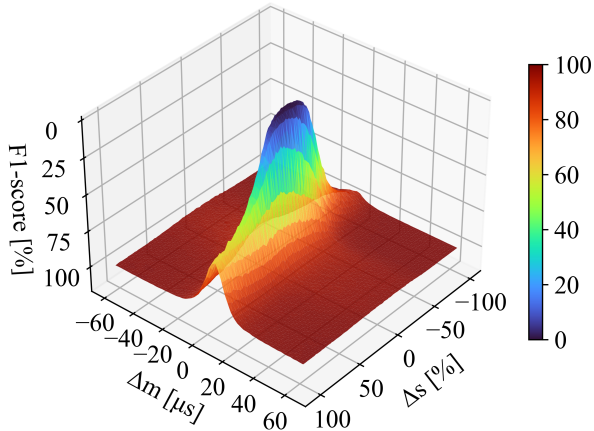


Fig. 6: F1-score of the MitM detection component in function of the alteration in F_{as} mean and variance due to the cyber attack.

the generated synthetic dataset, some malicious samples were indistinguishable from the legitimate ones, due to random choosing of Δm , Δs , and $\Delta \gamma_1$ values close to zero. In Fig. 6, the evaluation results for the second testbed IED with varying Δm and Δs are depicted. Similar consideration can be drawn for the first testbed vIEDs. As can be appreciated, the MitM detection method provided an F1-score higher than 99.9% down to an Δm variation of $20 \mu s$. This means that, to remain undetected, an attacker needs to alter the F_{as} measured by less than $20 \mu s$ on average. Moreover, even if a lower alteration is caused on the expected F_{as} mean, variations in the measured standard deviation or skewness of F_{as} still provide an information advantage to detect the ongoing MitM attack.

D. Attack Source Localization Evaluation

This last component was validated on network traffic acquired from the third testbed. To perform MitM attacks, each vIED in the HSR ring was compromised one at a time, its NICs' HSR bridge was disabled, and a C script was used to monitor, tamper, and forward SV frames. The network traffic was monitored and acquired with Wireshark at each vIED NIC during four experimental scenarios. Each experimental scenario consisted of one case representing normal operating conditions and five cases with a MitM attack in place in one vIED, thus leading to 24 acquisitions in total to be used for the training and testing of the DL model. As for the validation of the MitM detection component, measured F_{as} mean, standard deviation, and skewness were computed for each vIED, and then delivered to the attack source localization component. To further increase the realism of the experiments, the compromised vIED was allowed to report either normal or abnormal statistical metrics from both NICs. The DL model was trained on normal and anomalous cases from a subset of the experimental scenarios and then tested on normal and anomalous cases from different scenarios, as reported in Table V. This setup further demonstrates the generalization capabilities of the proposed DL-based method.

In fact, in a real deployment scenario, only normal operating conditions can usually be acquired from the field and used for training. However, as demonstrated in our experiments, the training set can be expanded with anomalous data acquired from an emulated network. The resulting trained model is then effective in detecting and localizing unseen MitM attacks in the real OT communication network. As reported in Table

TABLE V: Separation of scenarios among training and testing datasets.

Scenario ID	1	2	3	4
Training set	normal anomalous	-	normal anomalous	normal
Testing set	-	normal anomalous	-	anomalous

TABLE VI: Attack source localization results on the training and testing datasets.

	Accuracy	Precision	Recall	F1-score
Training set	99.810%	99.805%	99.807%	99.806%
Testing set	99.061%	99.096%	99.103%	99.099%

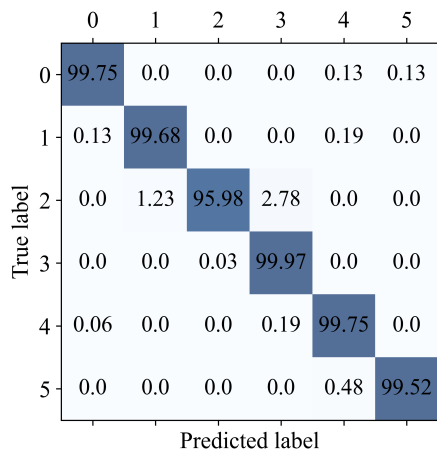


Fig. 7: Confusion matrix for attack source localization component on the testing set. Label “0” corresponds to normal conditions; labels “1” to “5” indicate which vIED is performing the MitM attack in the third testbed.

VI, the attack source localization method achieved accuracy, precision, recall, and F1-scores higher than 99% on both the training and testing datasets. Furthermore, as can be appreciated in Fig. 7, a FPR of 0.25% was obtained on the testing dataset. When the attack source was mislocalized, the error was most often confined to devices adjacent to the malicious one. This limits the number of devices that require further investigation after a cyber security incident.

E. Final Discussion and Considerations

Table VII summarizes the protection capabilities of different methods against the cyber attacks introduced in Section II-B. As can be appreciated, the method proposed in this paper addresses the limitations of conventional IDSs by effectively detecting and preventing more advanced attacks.

During flooding attacks, the proposed method discerns the legitimate and malicious frames and ensures that at most FS frames per second are received by the protected IED, thus drastically reducing the targeted device’s computational load and successfully mitigating the attack. While conventional IDSs can detect SV frames reception rate anomalies, they lack mechanisms to forward only legitimate frames to IEDs.

For replay attack injecting previously sniffed SV frames, the arrival PDF and replay protection module detects and discards duplicated $smcCnt$ values. Although alternative IDSs monitoring $smcCnt$ can identify such attacks, they cannot differentiate legitimate frames from malicious duplicates. Further, IDSs relying on current and voltage measurements monitoring remain ineffective because injected values may remain consistent with normal power system operation.

As shown in the quantitative analysis of the experimental scenarios, spoofing attacks are prevented by discarding the SV frames with the lowest legitimacy likelihood. The inherent difficulty of accurately and consistently estimating F_{as} prevents attackers from successfully mimicking legitimate traffic, thereby enabling effective detection and prevention of spoofing attacks. In contrast, other IDSs that rely on frame-

TABLE VII: Existing and proposed solutions’ protection capability against different types of attacks, where \checkmark denotes effective protection, \times ineffective protection, and \sim partial protection.

	(1)	(2)	(3)	(4)	(5)	(6)
Ustun et al. [14]	\times	\checkmark	\times	\times	\sim	\checkmark
Mo et al. [15]	\times	\checkmark	\times	\times	\sim	\checkmark
El Hariri et al. [16]	\times	\checkmark	\times	\times	\sim	\checkmark
Hussain et al. [17]	\times	\checkmark	\sim	\times	\sim	\checkmark
Hong et al. [18]	\sim	\times	\checkmark	\checkmark	\times	\times
Delhomme et al. [19]	\sim	\times	\times	\times	\times	\times
Wannous et al. [20]	\times	\times	\checkmark	\times	\times	\times
Hong et al. [21], [24]	\sim	\times	\checkmark	\times	\times	\times
Eynawi et al. [22]	\times	\times	\checkmark	\times	\times	\times
Manzoor et al. [23]	\times	\times	\checkmark	\checkmark	\times	\times
Our Solution	\checkmark	\checkmark	\checkmark	\checkmark	\checkmark	\checkmark

rate monitoring can detect spoofing when both legitimate and malicious SV streams are received, but they cannot distinguish which frames are legitimate.

High $smcCnt$ attacks, which trick replay protection by injecting frames with artificially elevated $smcCnt$ field values, are similarly thwarted because the frame arrival time constraints remain unsatisfied, causing malicious frames to be discarded.

During MitM attacks, where legitimate frames are dropped and malicious ones are injected at exactly FS frames per second, the arrival PDF and replay protection modules may initially accept malicious frames. However, the MitM detection module identifies the attack because matching the statistical properties, i.e., mean, variance, and skewness, of the legitimate SV stream presents substantial difficulty, particularly under realistic operating conditions. Prior IDS approaches cannot detect such attacks when the frame rate, $smcCnt$ field, SV stream identifier, and inter-frame timing are all properly emulated.

Finally, when SV frame authentication is enabled, but the pre-shared authentication key has been compromised, the proposed method’s arrival PDF and replay protection component detects and prevents attacks failing to satisfy the expected frame arrival time shift constraint, ensuring similar performances as during spoofing attack scenarios.

V. CONCLUSIONS

This paper presents a novel integrated hybrid statistical-deep learning-based method for detecting, preventing, and localizing IEC 61850 SV-based cyber attacks in digital substations. It has been shown that the statistical modeling of SV frames arrival time combined with DL enables the distinction between legitimate and malicious SV frames, early detection of MitM attacks on SV streams, and localization of malicious IEDs within the digital substation communication network. Experimental validation demonstrates promising intrusion detection, prevention, and localization performances while ensuring no interference to protection schemes in the absence of cyber attacks. The method satisfies IEC 61850-5 and IEC 61869-9 strict latency requirements and required throughput, respectively, and is robust to communication network latency, jitter, and time synchronization deviations. Thus, it provides a viable

solution to enhance cyber security and resilience in digital substations. Although validated on IEC 61850-compliant testbeds, future work will focus on field deployment in operational digital substations and defenses against advanced attacker strategies designed to evade frame acceptance filtering.

REFERENCES

- [1] D. U. Case, "Analysis of the cyber attack on the ukrainian power grid," *Electricity information sharing and analysis center (E-ISAC)*, vol. 388, no. 1-29, p. 3, 2016.
- [2] J. Slowik, "Crashoverride: Reassessing the 2016 ukraine electric power event as a protection-focused attack," *Dragos, Inc*, 2019.
- [3] P. Kozak, I. Klaban, and T. Šljajs, "Industroyer cyber-attacks on ukraine's critical infrastructure," in *2023 International Conference on Military Technologies (ICMT)*. IEEE, 2023, pp. 1–6.
- [4] C. Cimpanu, "Uk electricity middleman hit by cyber attack," 2024. [Online]. Available: <https://www.zdnet.com/article/uk-electricity-middleman-hit-by-cyber-attack/>
- [5] J. D. Christopher, "Sans 2024 state of ics/ot cybersecurity," *SANS Institute*, vol. 1, no. 7.1, pp. 7–2, 2024.
- [6] V. S. Rajkumar, M. Tealane, A. Ştefanov, A. Presekal, and P. Palensky, "Cyber attacks on power system automation and protection and impact analysis," in *2020 IEEE PES Innovative Smart Grid Technologies Europe (ISGT-Europe)*, 2020, pp. 247–254.
- [7] V. S. Rajkumar, A. Ştefanov, J. L. Rueda Torres, and P. Palensky, "Dynamical analysis of power system cascading failures caused by cyber attacks," *IEEE Transactions on Industrial Informatics*, vol. 20, no. 6, pp. 8807–8817, 2024.
- [8] S. M. S. Hussain, M. A. Aftab, S. M. Farooq, I. Ali, T. S. Ustun, and C. Konstantinou, "An effective security scheme for attacks on sample value messages in iec 61850 automated substations," *IEEE Open Access Journal of Power and Energy*, vol. 10, pp. 304–315, 2023.
- [9] J. Hong, R. Karnati, C.-W. Ten, S. Lee, and S. Choi, "Implementation of secure sampled value (sesv) messages in substation automation system," *IEEE Transactions on Power Delivery*, vol. 37, no. 1, pp. 405–414, 2022.
- [10] M. F. Elrawy, C. Fioravanti, G. Oliva, M. K. Michael, and R. Setola, "A geometrical approach to enhance security against cyber attacks in digital substations," *IEEE Access*, vol. 12, pp. 18 724–18 738, 2024.
- [11] M. Rodríguez, J. Lázaro, U. Bidarte, J. Jiménez, and A. Astarloa, "A fixed-latency architecture to secure goose and sampled value messages in substation systems," *IEEE Access*, vol. 9, pp. 51 646–51 658, 2021.
- [12] S. M. Suhail Hussain, "Lightweight optimized message authentication scheme for iec 61850 sampled value messages," *IEEE Transactions on Power Delivery*, vol. 39, no. 4, pp. 2552–2555, 2024.
- [13] J. Gaspar, T. Cruz, C.-T. Lam, and P. Simões, "Smart substation communications and cybersecurity: A comprehensive survey," *IEEE Communications Surveys & Tutorials*, vol. 25, no. 4, pp. 2456–2493, 2023.
- [14] T. S. Ustun, S. M. S. Hussain, L. Yavuz, and A. Onen, "Artificial intelligence based intrusion detection system for iec 61850 sampled values under symmetric and asymmetric faults," *IEEE Access*, vol. 9, pp. 56 486–56 495, 2021.
- [15] J. Mo and H. Yang, "Sampled value attack detection for busbar differential protection based on a negative selection immune system," *Journal of Modern Power Systems and Clean Energy*, vol. 11, no. 2, pp. 421–433, 2023.
- [16] M. El Hariri, E. Harmon, T. Youssef, M. Saleh, H. Habib, and O. Mohammed, "The iec 61850 sampled measured values protocol: Analysis, threat identification, and feasibility of using nn forecasters to detect spoofed packets," *Energies*, vol. 12, no. 19, 2019.
- [17] S. Hussain, S. M. S. Hussain, M. Hemmati, A. Iqbal, R. Alammari, S. Zanero, E. Ragaini, and G. Gruosso, "A novel hybrid cybersecurity scheme against false data injection attacks in automated power systems," *Protection and Control of Modern Power Systems*, vol. 8, no. 3, pp. 1–15, 2023.
- [18] J. Hong and C.-C. Liu, "Intelligent electronic devices with collaborative intrusion detection systems," *IEEE Transactions on Smart Grid*, vol. 10, no. 1, pp. 271–281, 2019.
- [19] A. Delhomme, L. Nweke, and S. Yildirim Yayilgan, "Detecting denial of service attacks in smart grids using machine learning: A study of iec 61850 protocols," in *Proceedings of the Eighteenth International Conference on Emerging Security Information, Systems, and Technologies (SECURWARE 2024)*, Nice, France, 2024, pp. 1–6.
- [20] K. Wannous, P. Toman, V. Jurák, and V. Wasserbauer, "Analysis of iec 61850-9-2le measured values using a neural network," *Energies*, vol. 12, no. 9, 2019.
- [21] J. Hong, C.-C. Liu, and M. Govindarasu, "Detection of cyber intrusions using network-based multicast messages for substation automation," in *ISGT 2014*, 2014, pp. 1–5.
- [22] A. Eynawi, A. Mumrez, G. Elbez, and V. Hagenmeyer, "Machine learning-based feature selection for intrusion detection systems in iec 61850-based digital substations," in *2024 IEEE International Conference on Communications, Control, and Computing Technologies for Smart Grids (SmartGridComm)*, 2024, pp. 1–7.
- [23] F. Manzoor, V. Khattar, C.-C. Liu, and M. Jin, "Zero-day attack detection in digital substations using in-context learning," in *2024 IEEE International Conference on Communications, Control, and Computing Technologies for Smart Grids (SmartGridComm)*, 2024, pp. 220–225.
- [24] J. Hong, C.-C. Liu, and M. Govindarasu, "Integrated anomaly detection for cyber security of the substations," *IEEE Transactions on Smart Grid*, vol. 5, no. 4, pp. 1643–1653, 2014.
- [25] H. Zhou, Y. Zheng, J. Xu, Y. Li, and J. Cao, "Propagation delay measurement and evaluation for sv based on hsr networks," *IEEE Transactions on Industrial Informatics*, vol. 18, no. 6, pp. 3970–3977, 2022.
- [26] N. Benvenuto and M. Zorzi, *Principles of Communications Networks and Systems*. John Wiley & Sons, 2011.
- [27] H. Kim and T. Shon, "Industrial network-based behavioral anomaly detection in ai-enabled smart manufacturing," *The Journal of Supercomputing*, vol. 78, no. 11, p. 13554, 2022.
- [28] S. Ali, J. Ara, and I. Shah, "A comparison of different parameter estimation methods for exponentially modified gaussian distribution," *Afrika Matematika*, vol. 33, no. 2, p. 58, May 2022.
- [29] J. Olivier and M. M. Norberg, "Positively skewed data: revisiting the box-cox power transformation," *International Journal of Psychological Research*, vol. 3, no. 1, pp. 68–95, 2010.